Check for updates

ADVANCED MATERIALS TECHNOLOGIES
www.advmattechnol.de

Dystrophic Muscle Affects Motoneuron Axon Outgrowth and NMJ Assembly

Ersilia Fornetti, Stefano Testa, Francesca De Paolis, Claudia Fuoco, Sergio Bernardini, Victorio Pozo Devoto, Gorazd Bernard Stokin, Sara Maria Giannitelli, Alberto Rainer, Anne Bigot, Carmine Zoccali, Jacopo Baldi, Doriana Sandonà, Roberto Rizzi, Claudia Bearzi, Giancarlo Forte, Stefano Cannata, and Cesare Gargioli**

The Neuromuscular Junction (NMJ) is a chemical synapse localized between the terminal branches of the spinal motor neurons and myofibers. In the past two decades coculture systems to generate the NMJ in culture are developed to address concerns about animal models, despite the complexity of its highly specialized structure makes the in vitro modeling a challenging task. Microfluidics, unlike mass cocultures, allow spatial and temporal control over different microenvironment by manipulating either neural cells or muscle cell populations independently. Therefore, exploiting an organ-on-a-chip approach, the aim is to obtain a reliable and predictive in vitro human model of NMJ in physiological and pathological conditions, to investigate the occurrence of synapse detriment in α-sarcoglycanopathy, a subtype of limb-girdle muscular dystrophy. For this purpose, motor neurons derived from human induced pluripotent stem cells (hiPSCs) and either healthy or α-sarcoglycan mutant human myogenic progenitors are seeded in two separated chambers of a microfluidic device. Differentiated myotubes and hiPSCs-derived motor neurons on-chip are able to establish points of interaction where pre- and postsynaptic structures colocalize. Moreover, the attraction of motor neurons axons by muscle fibers and the NMJ maturation appear to be affected by the muscular compartment, being impaired by the dystrophic cellular component.

1. Introduction

The chemical synapse at the Neuromuscular Junction (NMJ) presents a complex structure whose formation depends on the mutual induction of two main protagonists: spinal motor neurons and skeletal muscle fibers. An impairment of this delicate balance lies at the root of many neuromuscular diseases, whose cellular and molecular mechanisms are still partially unknown. This pathophysiological relevance has generated in many research groups the keen interest in developing valid study models: for decades animal models, especially mice, have been the gold standard for neuromuscular disease modeling.[1] In general, animal models capture important hallmarks of their human disease counterparts and thus are invaluable for understanding disease progression on an organ and organism scale. However, the adequate clinical translation of this findings in human pathophysiology

E. Fornetti, S. Testa, F. De Paolis, C. Fuoco, S. Bernardini, S. Cannata, C. Gargioli
Department of Biology
Rome University Tor Vergata
Rome 00133, Italy
E-mail: cannata@uniroma2.it; cesare.gargioli@uniroma2.it

V. Pozo Devoto, G. B. Stokin, G. Forte
International Clinical Research Center (ICRC)
St Anne's University Hospital
Brno CZ-65691, Czech Republic

S. M. Giannitelli, A. Rainer
Department of Engineering
Università Campus Bio-Medico di Roma
Rome 00128, Italy

The ORCID identification number(s) for the author(s) of this article can be found under https://doi.org/10.1002/admt.202101216.

© 2022 The Authors. Advanced Materials Technologies published by Wiley-VCH GmbH. This is an open access article under the terms of the Creative Commons Attribution License, which permits use, distribution and reproduction in any medium, provided the original work is properly cited.

DOI: 10.1002/admt.202101216

A. Rainer
Institute of Nanotechnology (NANOTEC)
National Research Council
Lecce 73100, Italy

A. Bigot
Center of Research in Myology
INSERM
Institute of Myology
Sorbonne University
Paris 75013, France

C. Zoccali, J. Baldi
IRCCS Regina Elena National Cancer Institute
Rome 00144, Italy

C. Zoccali
Department of Anatomical, Histological, Forensic Medicine and Orthopedic Science
University of Rome La Sapienza
Rome 00185, Italy

D. Sandonà
Department of Biomedical Sciences
University of Padua
Padua 35131, Italy

2365709x, 2022, 7, Downloaded from https://onlinelibrary.wiley.com/doi/10.1002/admt.202101216 by CochraneItalia, Wiley Online Library on [06/12/2024]. See the Terms and Conditions (https://onlinelibrary.wiley.com/terms-and-conditions) on Wiley Online Library for rules of use; OA articles are governed by the applicable Creative Commons License

have so far failed: none of the potential drugs tested on animal models has proven equally successful in humans.[2] In fact, current animal models available for many diseases involving NMJ integrity and signaling derangement only replicates a portion of the phenotype spectrum in the human diseases, making it difficult to predict the therapeutic outcome in humans.[3] Another interesting element adding to these aspects regards recent findings about distinctive features of the human NMJ that differ widely from the murine synapse: human NMJs are indeed significantly smaller, less complex and more fragmented than the well-known pretzel-like-shaped murine NMJs.[4] Surprisingly, there are also differences in their molecular composition, as revealed by proteomic analysis, and in the active zone proteins localization at the innervation site. This suggests that relying only on murine studies to assume human synapse characteristics may not be an entirely appropriate strategy.

In an attempt to overcome the obstacles due to the inability of animal models to fully mimic human diseases and to the morphological and molecular differences among human and murine NMJs, numerous research groups focused on trying to recreate the human NMJ using in vitro models for more personalized high-throughput analysis. Due to the complexity of the NMJ, recreating the right conditions for synaptogenesis in vitro is undoubtedly a challenging task. In the past few decades, different strategies have been adopted to obtain the combination of motor neurons and skeletal muscle fibers culture. The majority of these approaches utilizes mass coculture, in which both cell populations are mixed on the same culture platform and maintained with the same culture medium.[5] These studies were fundamental to widen our knowledge about motor neurons and skeletal muscle fibers in vitro coculture. However, mass cocultures do not provide fully suitable conditions for the formation of a mature NMJ as evidenced by image analysis revealing blotched pre- and postsynaptic markers colocalization and poor acetylcholine receptor clustering in mass cocultures as compared to native NMJs.[5,6] In fact, a key factor to be considered for in vitro modeling is the cell configuration to be anatomically relevant and eligible for measuring functional phenotypes.[7] As in physiological conditions motor neurons soma are located in the spinal cord and only axons directly interact with muscle fibers, seeding motor neurons on top of myotubes may not be anatomically correct and might alter the physiology of one or both cell types.

Microfluidics and the organ-on-chip approach turned out to be ideal to study axonal biology,[8] providing a novel platform especially effective for the NMJ in vitro modeling. In fact, by giving the opportunity to coculture motor neurons and muscle fibers in separated chambers connected by axons passing through microchannels, it allows a precise control over the cell microenvironments.[2] As compared to conventional in vitro mass coculture, microfluidics allows to coculture different cell types with different media, ideal condition for providing each cell type with growth and differentiation factors specific for their needs. Moreover, microfluidic platforms allow for precise, specific, and localized interrogation of the system, giving the opportunity to isolate the field of analysis either at the soma, along the axons or at the neuromuscular junction. Over the past decade, microfluidics has been exploited to develop NMJ-on-chip models with different origin cells. In particular, the majority of these culture systems have been developed by using animal cells which cannot be considered as fully relevant in terms of human physiology, but can provide important proof-of-concept and basic physiological information. Publications related to the development of the NMJ in microfluidic devices demonstrated that in these culture systems is indeed possible to detect the key components of the NMJ,[9–11] to perform both morphological [11,12] and functional analyses,[13–15] to reproduce diseased phenotypes,[16] to treat cocultures with drugs or toxins,[13,15,16] and to study the molecular mechanisms leading to the development of pathologies.[15,17] What is still missing from these promising achievements is the more in-depth and exhaustive analyses of both morphological and functional parameters, which are needed to confirm the reliability of NMJs models. Moreover, the knowledge acquired from these publications should lay the groundwork for the development of diseased models employing human patient-specific cells to be used for the investigation of the pathological mechanisms underlying NMJ damage and neurodegenerative diseases.[18–20] In particular, the study of the NMJ contribution in muscular dystrophies progression is still poorly explored as compared to other neuromuscular disorders and would widely benefit from the microfluidics approach. The NMJ pathological derangement has been characterized in the Duchenne Muscular Dystrophy (DMD) and pointed out numerous differences in the structure, function, and gene expression between the healthy and pathologic condition.[21] However, a similar characterization is still totally lacking for other less common types of muscular dystrophies such as sarcoglycanopathies, which comprise four subtypes of autosomal recessive limb-girdle muscular dystrophies (LGMD). Among these, the most frequent subtype is α-sarcoglycanopathy (LGMD2D) which is caused by the α-sarcoglycan (α-SG) mutated protein.[22] The pathology is characterized by the progressive proximal weakness of the shoulder and pelvic girdle muscles upon childhood onset, resulting in difficulty walking, scapular winging, calf hypertrophy, and Achilles tendon contractures.[23] Interestingly, a novel function of α-SG in NMJ stabilization during aging has recently emerged, consisting in delaying the ubiquitination of LRP4, a receptor of agrin that is crucial for NMJ formation and maintenance.[24] However, the contribution of the α-SG mutant to the NMJ derangement in the disease progression is largely unexplored.

As the field advances, models of neuromuscular tissues on-chip progressively demonstrate how, in combination with animal models, they could potentially be considered as complementary tools for modeling multiple aspects of neuromuscular diseases for identifying new therapeutic strategies.[7] By exploiting microfluidics and organ-on-chip technologies, the aim of this work is to reproduce the human neuromuscular junction in vitro to possibly identify defects in the neural and muscular cross-talk affecting NMJ formation in a α-sarcoglycanopathy model. For this purpose, motor neurons

R. Rizzi, C. Bearzi
Fondazione Istituto Nazionale di Genetica Molecolare
Milan 20122, Italy
R. Rizzi, C. Bearzi
Institute of Genetic and Biomedical Research
UOS of Milan
National Research Council (IRGB-CNR)
Milan 20138, Italy

© 2022 The Authors. Advanced Materials Technologies published by Wiley-VCH GmbH

2365709x, 2022, 7, Downloaded from https://onlinelibrary.wiley.com/doi/10.1002/admt.202101216 by CochraneItalia, Wiley Online Library on [06/12/2024]. See the Terms and Conditions (https://onlinelibrary.wiley.com/terms-and-conditions) on Wiley Online Library for rules of use; OA articles are governed by the applicable Creative Commons License

derived from human iPSCs and skeletal muscle fibers derived from human myogenic progenitors are seeded in two separated chambers of a microfluidic device. The two sides of the devices are linked through microchannels that enable the axonal outgrowth toward the muscle side, but not cell bodies migration. The setup was designed as a reliable platform that is suitable for hosting patient-specific cells and to perform functional and molecular analysis on the effect of the muscle cells genotype on axonal growth and NMJ formation.

2. Results

2.1. Differentiation of Functional Spinal Motor Neurons From Human iPSCs

To test the quality of human motor neurons obtained from iPSCs-derived neural progenitors, cells were cultured for 15 days with neural optimized medium (NOM) supplemented with 50×10^{-9} M retinoic acid (RA) and 50 ng mL^{-1} sonic hedgehog (SHH). Cell differentiation was evaluated through immunofluorescence analysis by a combination of antibodies directed against well-known neural differentiation markers (**Figure 1**A). Differentiated cells demonstrated strong positivity for the motor neuron-specific marker HB9 (percentage of HB9+ nuclei over total: 93.86 ± 6.4%), the axonal marker phospho-neurofilament (pNF), the nuclear marker NeuN, the dendritic marker MAP2, and the generic neural marker Tau. Motor neuron cultures also showed some heterogeneity and to be enriched with GFAP-positive cells, an astrocyte marker. The presence of astrocytes, which offer both structural and metabolic neuron support, is considered to be beneficial when their percentage in culture remains low and does not overgrow motor neurons.[25]

After confirming the motor neuron differentiation through image analysis, to test whether these cells were also functional, iPSCs-derived neural progenitors were directed toward motor neuron differentiation in a 96-well multielectrode array plate for up to 30 days (Figure 1B). The obtained results demonstrated that iPSCs-derived motor neurons not only are able to spontaneously generate spikes, which indicate a general electrical activity, but they also produce bursts (series of at least 5 spikes in less than 100 ms), which are considered a sign of electrophysiological maturity. Starting from day 10 of differentiation, the electrodes of each well began to simultaneously detect spikes and bursts within the culture, meaning that connected networks were being formed through synapses among motor neurons. A significant aspect emerged from the analysis is that the peak of activity for all the parameters examined was reached around day 15 from plating, an interesting information to determine the coculture experiments timing.

2.2. Skeletal Muscle Differentiation From hMSCs and From hTERT/CDK4 Human Immortalized Myoblasts

In order to evaluate skeletal muscle differentiation potential of skeletal muscle-derived human Mesenchymal Stem Cells (hMSCs), cells were cultured for 15 days in the presence of growth medium. No specific differentiation factors were added, as skeletal muscle-derived hMSCs are able to spontaneously form myotubes upon reaching 80% confluence.[26] At the given time point, immunofluorescence analysis was performed by using antibodies raised against the terminal muscle differentiation marker myosin heavy chain (MHC). Image analysis confirmed that hMSCs were able to produce large MHC-positive syncytia containing numerous nuclei in vitro (**Figure 2**A). Similarly, immortalized myoblasts from either healthy donors or α-sarcoglycanopathy-suffering patients (α-SG myoblasts) were cultured for 15 days in a 6-well plate with differentiation medium supplemented with 10 mg mL^{-1} insulin. The results demonstrated that both healthy and α-SG immortalized myoblasts were able to differentiate with high efficiency in MHC-positive myotubes (Figure 2A). Moreover, the high differentiation efficiency was found to be comparable in the three muscle progenitor types employed, as emerged from the fusion index analysis which did not show any statistically significant difference (Figure 2B). However, a deeper analysis of the distribution of myogenic nuclei revealed a significant prevalence of myotubes containing more than 5 nuclei in healthy myotubes (from hMSCs and healthy immortalized myoblasts), indicating a greater presence of larger and more mature myotubes; conversely, α-SG-derived cells, differentiate into small myotubes containing mainly between 2 and 5 nuclei (Figure 2C). The evidence of a more immature phenotype in α-SG myotubes as compared to their healthy counterpart, was also confirmed by the calculation of myotubes thickness in both conditions, being significantly lower in α-SG myoblasts-derived myotubes (Figure 2D).

2.3. Fluorescent BTX-Staining on Skeletal Muscle Prepatterned AChRs

At early stages of NMJ development, acetylcholine receptors (AChR) are known to be prepatterned along the sarcolemma of the developing muscle fibers independently of neural signals.[28] In order to investigate whether this process is also conserved in vitro and to observe the presence and the organization of AChRs on differentiated myofibers, hMSCs and immortalized myoblasts were differentiated and analyzed through immunofluorescence staining, using murine satellite cells as control (**Figure 3**). In particular, to detect the AChRs on the myotubes membrane, fluorescent α-bungarotoxin (BTX, an AChRs-binding toxin) was employed. In accordance with what reported in literature,[28] AChRs on the membrane of muscle cells cultured in the absence of motor neurons appear scattered along the sarcolemma, without a specific organization (as shown in Figure 3 for human-derived myotubes). Interestingly though, myotubes differentiated from murine satellite cells seemed to have a more organized arrangement of AChRs, which was concentrated in narrow regions of the muscle fiber (Figure 3). Although this aspect has emerged also form other studies,[29] it still lacks proper insights. These results suggest that murine muscle cells may have a natural predisposition in clustering the AChRs even in absence of neural signals, explaining why it is way easier to obtain NMJs in vitro models employing murine cells.

© 2022 The Authors. Advanced Materials Technologies published by Wiley-VCH GmbH

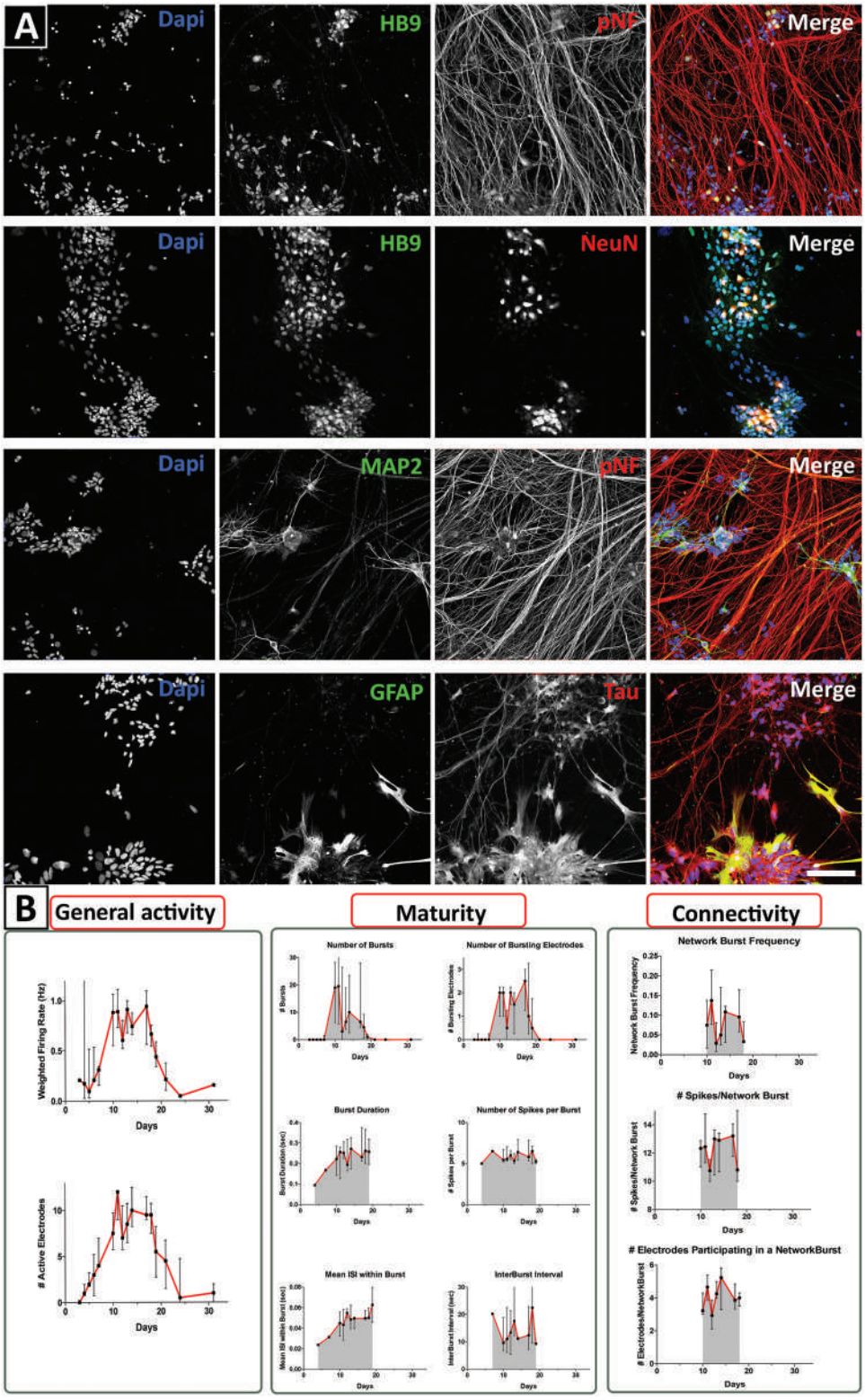

Figure 1. iPSCs-derived motor neurons characterization. A) Human motor neurons cultures at day 15 after seeding, showing expression of the specific nuclear marker HB9, formation of a correct polarization with pNF-positive axons and MAP2-positive dendrites, positivity for the generic neural markers NeuN and Tau, and a low percentage of GFAP-positive astrocytes. Scale bar: 100 µm. B) MEA analysis during maturation of human motor neurons from day 0 (seeding) to day 30. The general electrical activity was determined as the increase in weighted fire rate (average of normalized values calculated by dividing the number of spikes detected by an active electrode by the unit of time of 120 s) and number of active electrodes. Cell maturity was determined as the increase in the number of bursts detected by an electrode, number of electrodes detecting bursts, burst duration, number of

© 2022 The Authors. Advanced Materials Technologies published by Wiley-VCH GmbH

2365709x, 2022, 7, Downloaded from https://onlinelibrary.wiley.com/doi/10.1002/admt.202101216 by CochraneItalia, Wiley Online Library on [06/12/2024]. See the Terms and Conditions (https://onlinelibrary.wiley.com/terms-and-conditions) on Wiley Online Library for rules of use; OA articles are governed by the applicable Creative Commons License

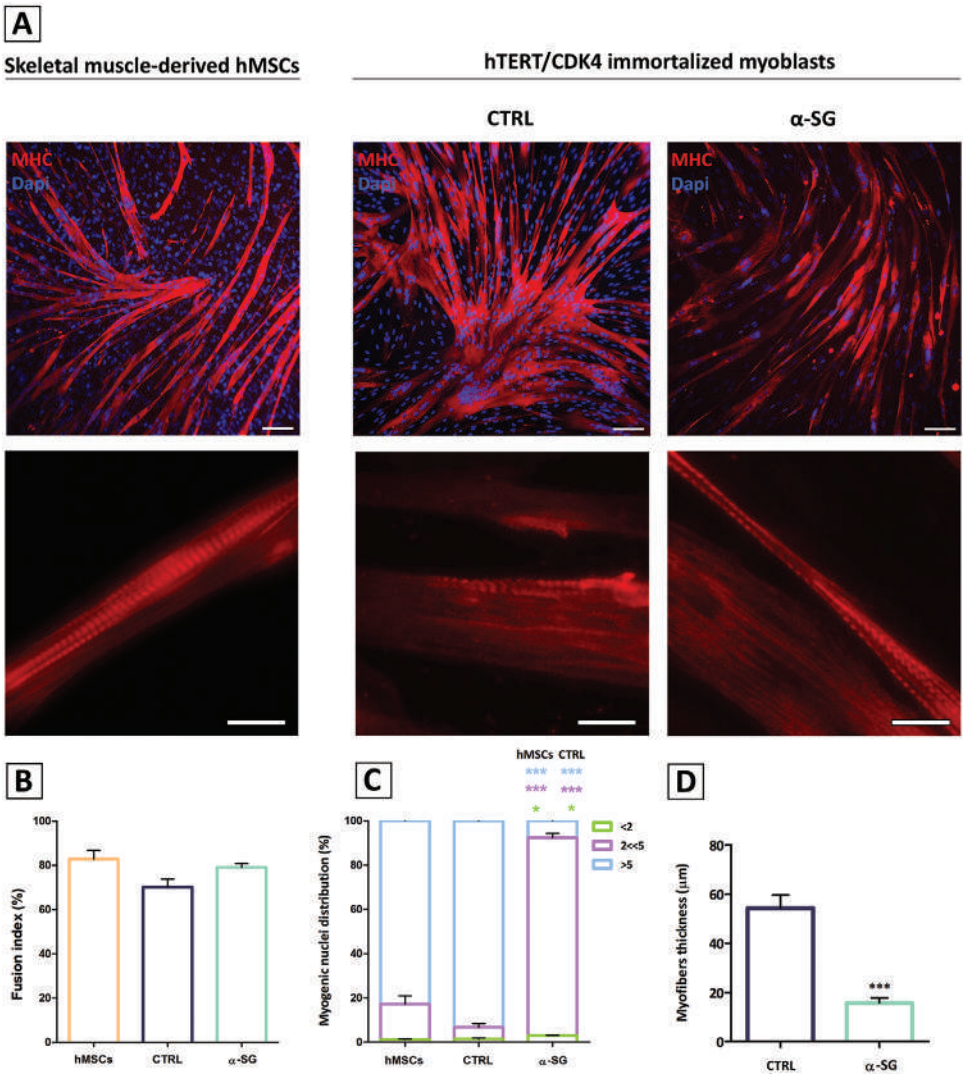

Figure 2. Differentiation of human muscle progenitors. A) Skeletal muscle-derived hMSCs, immortalized healthy (CTRL) and α-sarcoglycan mutant (α-SG) myoblasts show proper formation of myotubes expressing the skeletal muscle differentiation marker MHC (top row) and presenting sarcomere striations (bottom row) at day 15 of differentiation; nuclei were counterstained by Dapi. Top row scale bars: 100 µm. Bottom row scale bars: 20 µm. B) Fusion Index bar plot representation for myotubes obtained from muscle-derived hMSCs, CTRL and α-SG myoblasts, showing no statistically significant difference in their differentiation efficiency (n = 9 analyzed fields from 3 independent experiments per cell type). One-way ANOVA Tukey's Multiple Comparison Test was performed. C) Bar plot representation of the myogenic nuclei distribution calculated as the percentage of nuclei inside mononuclear myotubes (<2), the percentage of nuclei inside myotubes containing between 2 and 5 nuclei (2 << 5) and the percentage of nuclei inside myotubes containing more than five nuclei (>5), according to Mozzetta et al.[27] (n = 9 analyzed fields from 3 independent experiments per cell type). One-way ANOVA Tukey's Multiple Comparison Test was performed. *p < 0.02, **p < 0.002, ***p < 0.0001 D) Bar plot representation of myofibers thickness in CTRL and α-SG differentiation. Phenotypic difference between CTRL and α-SG myotubes is evidenced by a significant lower thickness in diseased myotubes (3.6-fold) (n = 9 analyzed fields from 3 independent experiments per cell type. A minimum of 10 myotubes per field were analyzed.) ***p < 0.0005.

2.4. Coculture of hMSCs and hiPSCs-Derived Motor Neurons in A Microfluidic Device

After characterizing the cellular components of the coculture independently, in order to observe the bidirectional communication between motor neurons and muscle cells, iPSCs-derived neural progenitors and muscle-derived hMSCs were plated in the two separated compartments of a commercially available microfluidic device (XonaMicrofluidics, RD450). The microchannels separating the two compartments, with a total length of

spike/burst, burst inter spikes interval (ISI, a parameter that determines bursts duration: grater the interval longer the burst, yet within 100 ms) and inter burst interval. Network connectivity was determined as the increase in network burst frequency, number of spikes/network burst and number of electrodes participating in a network burst.

© 2022 The Authors. Advanced Materials Technologies published by Wiley-VCH GmbH

2365709x, 2022, 7, Downloaded from https://onlinelibrary.wiley.com/doi/10.1002/admt.202101216 by CochraneItalia, Wiley Online Library on [06/12/2024]. See the Terms and Conditions (https://onlinelibrary.wiley.com/terms-and-conditions) on Wiley Online Library for rules of use; OA articles are governed by the applicable Creative Commons License

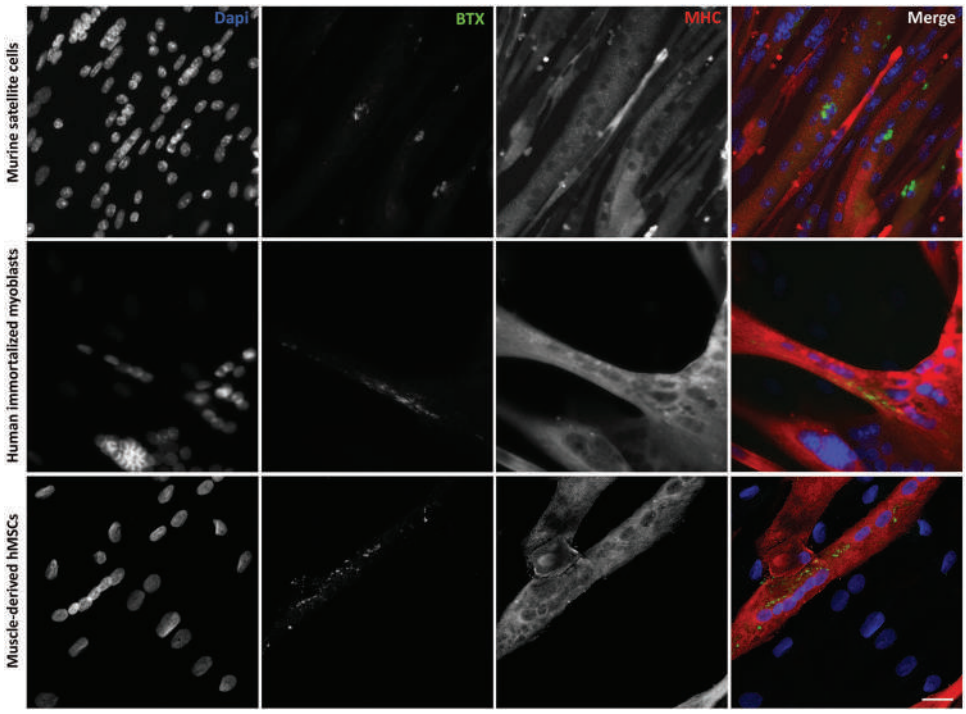

Figure 3. AChRs prepattering analysis on differentiated myotubes. Fluorescent-BTX comparative staining revealing a scattered arrangement of AChRs along the sarcolemma of human-derived myotubes, as described in literature,[28] and a more organized pattern of the receptors on murine-derived myotubes. Scale bar: 25 µm.

450 µm, has previously been reported to promote polarized growth of motor neurons, with dendrites remaining confined to the neural compartment and only axons extending into the microchannels toward the muscle compartment.[30] Thanks to the microfluidic coculture configuration, each cell type was maintained throughout the maturation in its specific differentiation medium. Starting from the day after seeding, neural progenitors began to undertake motor neural differentiation and developed neural processes (**Figure 4**). On the other side, after a period of proliferation lasting about 3 days, hMSCs started to fuse and differentiate spontaneously into skeletal muscle. At day 7, neurites reaching the muscle compartment through the microchannels and contacting the differentiated myotubes could be noticed. After 15 days, a mature coculture with numerous axons sprouting toward the muscle compartment and the formation of large myotubes was established (Figure 4). As a confirmation that the microfluidic device is suitable for an optimal cell growth and maturation, spontaneous muscle twitching events were recorded (Video S1, Supporting Information).

Interestingly, when motor neurons have been cultured in the microfluidic device with the distal compartment being filled with muscle medium only, they initially grew throughout the microchannels and extended in the distal chamber, while abruptly retreating in the following days. As a result, no axon could be detected in the distal compartment at day 15 (Figure S1, Supporting Information). These results indicate that the presence of muscle cells in the distal compartment facilitates the extension and the maintenance of axons, suggesting the secretion of neurotrophic factors from the muscular component is needed for this process.

2.5. Identification of Bona Fide NMJs Within the Microfluidic Coculture

At day 15 of co-culture, the microfluidic chambers were analyzed through immunofluorescence to confirm differentiation in both cell types and to possibly identify bona fide NMJs at the contact points between motor neurons and myotubes, as already noticed in brightfield images. Differentiated motor neurons resulted positive for the neural markers βIII tubulin and pNF, while differentiated myotubes showed the ability to express the skeletal muscle markers desmin and MHC (**Figure 5**; and Figure S2, Supporting Information). Numerous regions of the muscle compartment were identified showing interaction points between motor neurons and muscle cells (Figure 5B,C). Most importantly, the colocalization of motor neuron axons with the presynaptic marker synaptophysin (Syn) and fluorescent BTX-binding AChRs on the myotubes was highlighted (**Figure 6**). This evidence is of particular relevance because the copresence of these three elements suggests a bidirectional induction between the two cell types and the formation of bona fide NMJs.

2.6. Muscle Cells Affect Motor Neuron Mitochondria Redistribution and Motility

In order to study some key functional aspects of the coculture biology, motor neurons metabolic activity was evaluated through axoplasm mitochondrial motility analysis in both microfluidic cocultures and in control chips with motor neuron

© 2022 The Authors. Advanced Materials Technologies published by Wiley-VCH GmbH

2365709x, 2022, 7, Downloaded from https://onlinelibrary.wiley.com/doi/10.1002/admt.202101216 by CochraneItalia, Wiley Online Library on [06/12/2024]. See the Terms and Conditions (https://onlinelibrary.wiley.com/terms-and-conditions) on Wiley Online Library for rules of use; OA articles are governed by the applicable Creative Commons License

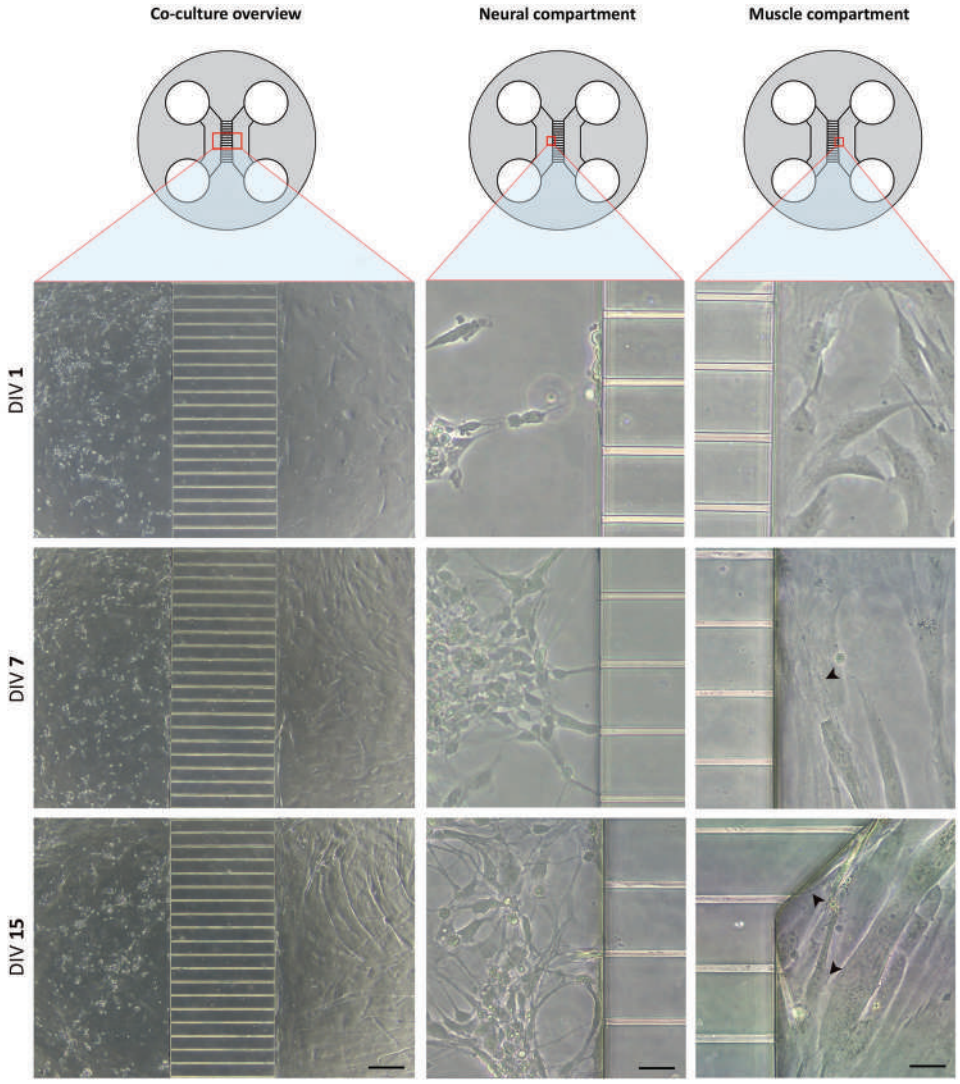

Figure 4. Human motor neurons and hMSCs co-culture in the two-compartment microfluidic chip. Coculture overview and magnified neural and muscle compartments brightfield images at different time points (DIV, day in vitro). Progressive growth and differentiation of both iPSCs-derived motor neurons and hMSCs-derived myotubes, with a well-established mature coculture at day 15. Black arrows indicate axons protruding from the microchannels and contacting differentiated myotubes. Coculture overview scale bar: 150 µm. Neural and muscle compartments scale bar: 30 µm.

monocultures. MitoTracker Green FM-dyed mitochondria were tracked at the interface between the neural compartment and microchannels entrance through live image analysis (**Figure 7**A), and kymographs were generated from recordings (refer to the Experimental Section). Obtained kymographs were accordingly used to measure mitochondrial velocity, motile mitochondria percentage and anterograde shift percentage in both conditions. All these functional parameters resulted significantly enhanced in motor neurons cocultured with muscle cells, suggesting that the presence of the muscle component in the distal compartment affects motor neurons mitochondria redistribution and motility (Figure 7). Notably, although the kymographs show an oscillatory mitochondria movement, a percentage greater than 70% of net anterograde shift in coculture-grown motor neurons indicate that nearly all tracked mitochondria are transported from the soma to the terminal end of the growth cone, implying this is the area with the highest metabolic demand (Figure 7B,C). This phenomenon is well-known to take place during axons active growth and NMJ formation.[31–33]

2.7. Muscle Cell Phenotype Affect Motor Neuron Elongation

After determining that human iPSCs-derived motor neurons and human muscle progenitors can be successfully cocultured in a two-chamber microfluidic chip, more in-depth analyses were performed exploiting a diseased muscle phenotype. iPSCs-derived neural progenitors and immortalized myoblasts from both healthy-donors (CTRL) and α-sarcoglycanopathy-suffering patients (α-SG) were plated in the two separated compartments of the microfluidic chip. At day 15, the microfluidic cocultures were

© 2022 The Authors. Advanced Materials Technologies published by Wiley-VCH GmbH

2365709x, 2022, 7, Downloaded from https://onlinelibrary.wiley.com/doi/10.1002/admt.202101216 by CochraneItalia, Wiley Online Library on [06/12/2024]. See the Terms and Conditions (https://onlinelibrary.wiley.com/terms-and-conditions) on Wiley Online Library for rules of use; OA articles are governed by the applicable Creative Commons License

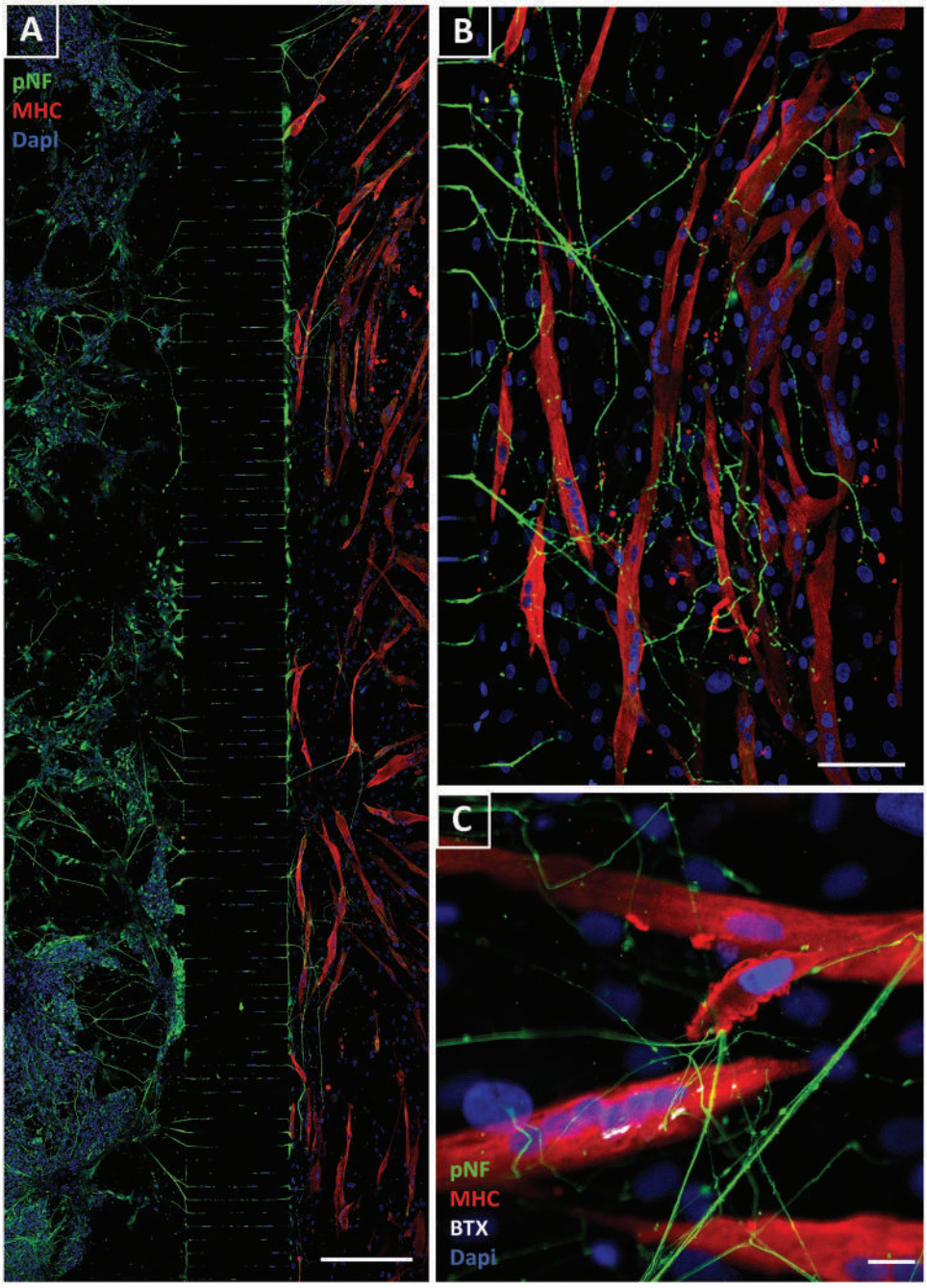

Figure 5. Immunofluorescence analysis on microfluidic chip cocultures. A) Confocal large-scale image showing the reconstruction of the entire coculture chip. Scale bar: 400 µm. B) Magnified image of the muscle compartment showing extensive interaction regions between motor neurons and myotubes. Scale bar: 50 µm. C) Higher magnification images demonstrated the colocalization of the fundamental components of the NMJ: pNF-positive motor neurons, MHC-positive myotubes and fluorescent-BTX-binding AChRs. Scale bar: 20 µm.

examined through immunofluorescence analysis (**Figure 8**A) and morphological parameters were evaluated in both conditions. The extent of motor neuron recruitment in the muscle compartment, indicated as neural elongation, was evaluated by calculating the percentage of microchannels crossed by axons and the total length covered by motor neurons per field (Figure 8B). The values of both parameters resulted remarkably reduced (6-fold and 25-fold, respectively) in α-SG as compared to CTRL cocultures. Conversely, to test whether the presence of the motor neurons in the proximal compartment has a positive effect on muscle differentiation, fusion index analyses were performed on differentiated healthy and α-SG-derived myotubes in monoculture and in microfluidic coculture. This analysis showed no significant changes occurred in cocultures of healthy and diseased cells as compared to control monocultures. Similarly, myotubes thickness, which is considered an index of maturation,[34]

© 2022 The Authors. Advanced Materials Technologies published by Wiley-VCH GmbH

2365709x, 2022, 7, Downloaded from https://onlinelibrary.wiley.com/doi/10.1002/admt.202101216 by CochraneItalia, Wiley Online Library on [06/12/2024]. See the Terms and Conditions (https://onlinelibrary.wiley.com/terms-and-conditions) on Wiley Online Library for rules of use; OA articles are governed by the applicable Creative Commons License

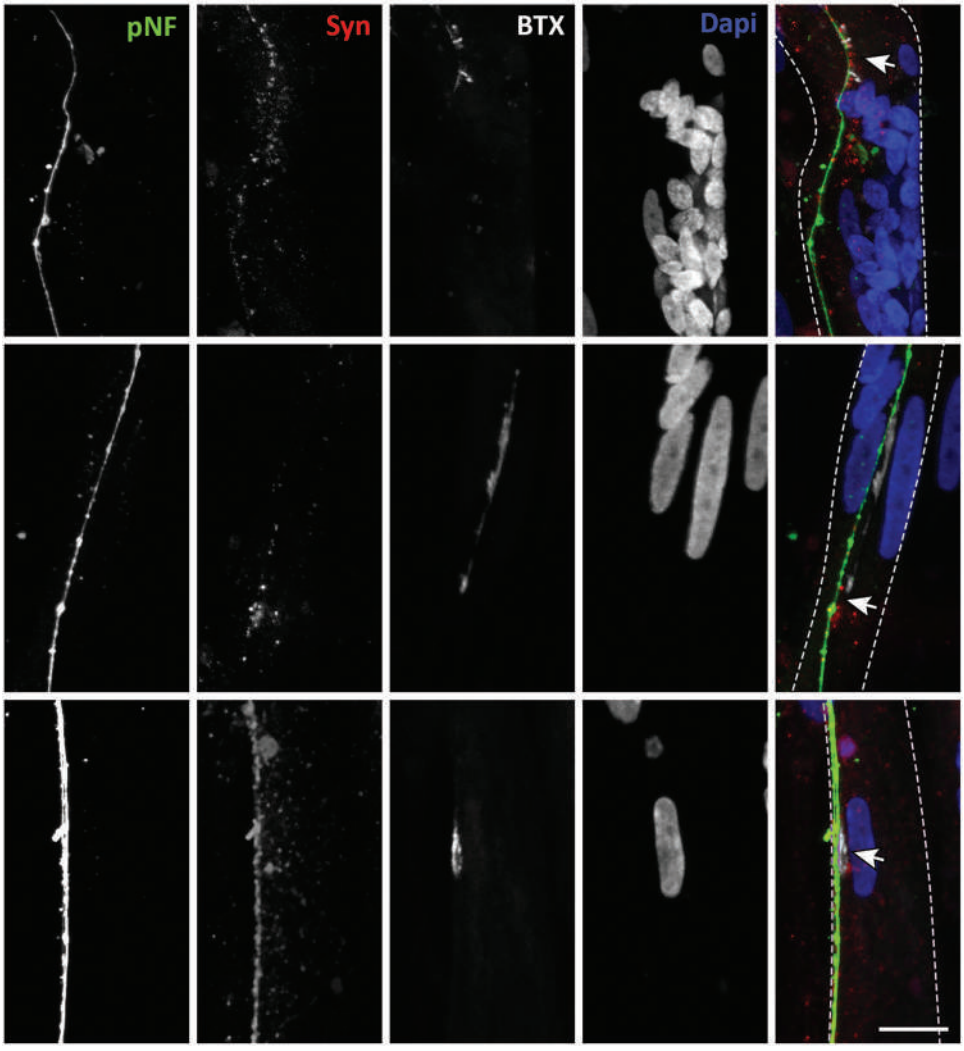

Figure 6. Pre- and postsynaptic marker analysis. Representative immunostaining images of the contact points between motor neurons and myotubes, with the colocalization of Syn and fluorescent BTX-binding AChRs. Dashed lines trace myotube outline. Scale bar: 20 µm.

did not undergo significant variations between monocultures and cocultures, both in CTRL and α-SG myotubes. Altogether, these results suggest that while muscle cell phenotype seems to strongly affect motor neurons recruitment, motor neurons do not play a significant role in muscle differentiation efficiency, nor in myotubes size. Moreover mitochondrial motility analysis was carried out by comparing healthy and α-SG cocultures (Figure S3, Supporting Information). As a result, the diseased phenotype does not appear to affect mitochondrial velocity and motile mitochondria percentage between the two models. However, while a significantly predominant anterograde movement was obtained in the axoplasms of CTRL cocultures (according with the hMSCs coculture experiments), in α-SG cocultures motile mitochondria do not show a predominant directionality.

2.8. Density and Shape Analysis on BTX-Binding AChRs Clusters

To test whether motor neurons are indeed able to promote AChRs clustering in vitro, as occurs in physiological conditions during the formation of the NMJ,[28,35] more focused analyses were performed on BTX-binding AChRs arrangement and density. Number, size, and circularity of AChRs clusters were calculated in defined ROIs (2500 µm^2) of myotubes differentiated in control monocultures and myotubes differentiated in microfluidic cocultures from both CTRL and α-SG myoblasts (**Figure 9**). A higher cluster aggregation in coculture-grown myotubes resulted in significantly fewer but larger clusters, with an intermediate effect in α-SG cocultures (slightly greater number and slightly smaller size) as compared to CTRL cocultures, although this difference was not statistically significant. Circularity index, a parameter ranging from 0 to 1 and describing the shape of an object through the area/perimeter ratio, was found to be significantly closer to 1 in both CTRL and α-SG cocultures compared to the monoculture. In this case, the effect observed in CTRL coculture-grown myotubes is statistically significant also compared to the α-SG coculture-grown myotubes and indicate that healthy AChRs clusters have a circular shape more similar to the nummular structure described in the literature for the human NMJ.[4]

© 2022 The Authors. Advanced Materials Technologies published by Wiley-VCH GmbH

2365709x, 2022, 7, Downloaded from https://onlinelibrary.wiley.com/doi/10.1002/admt.202101216 by CochraneItalia, Wiley Online Library on [06/12/2024]. See the Terms and Conditions (https://onlinelibrary.wiley.com/terms-and-conditions) on Wiley Online Library for rules of use; OA articles are governed by the applicable Creative Commons License

2365709x, 2022, 7, Downloaded from https://onlinelibrary.wiley.com/doi/10.1002/admt.202101216 by CochraneItalia, Wiley Online Library on [06/12/2024]. See the Terms and Conditions (https://onlinelibrary.wiley.com/terms-and-conditions) on Wiley Online Library for rules of use; OA articles are governed by the applicable Creative Commons License

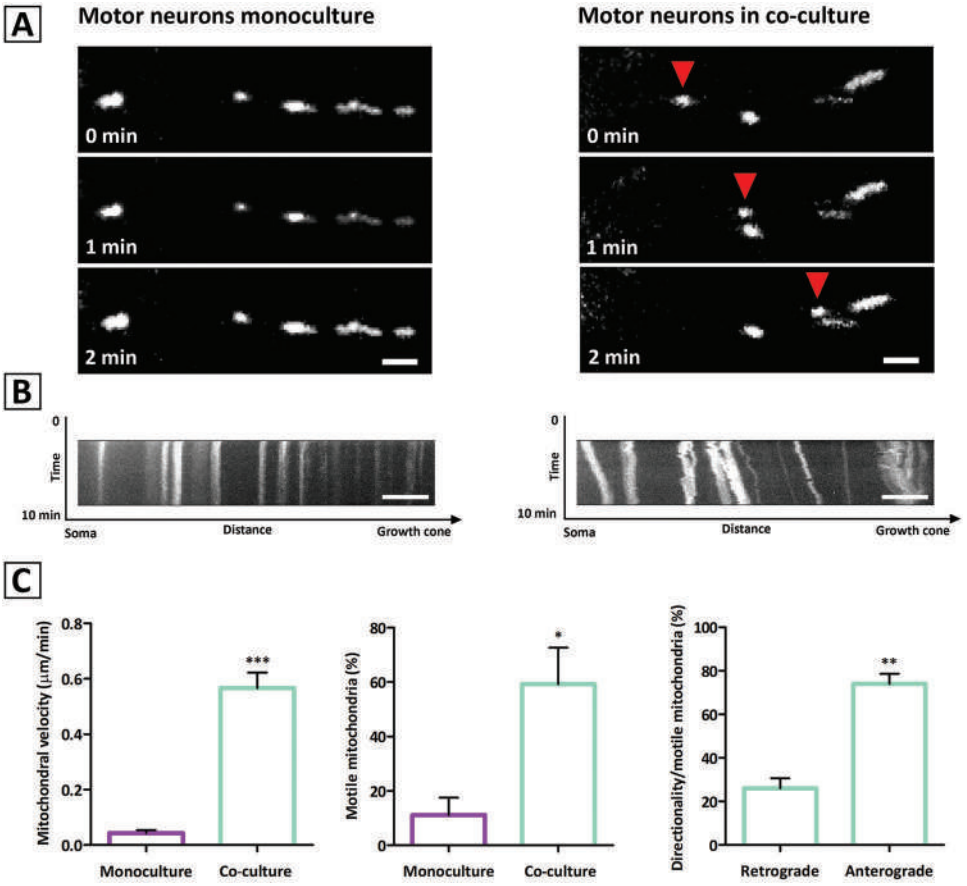

Figure 7. Axoplasm mitochondrial activity analysis. A) Time-lapse images obtained from fluorescent-dyed mitochondria tracking show how their position changes over time in the axons of motor neurons cocultured with muscle cells, while remaining rather motionless in control motor neurons monocultures. Scale bar: 3 µm. B) Kymographs obtained from time-lapse recordings, in which each band identifies a single mitochondrion. The band is expected to be perpendicular to the *x*-axis for stationary particles, while being shifted toward growth cone direction for particles undergoing anterograde movement or toward soma direction for retrograde movement. In control monoculture bands appear stationary, while they show a clear anterograde shift in coculture-grown motor neurons. Scale bar: 15 µm. C) Mitochondrial velocity and percentage of motile mitochondria resulted significantly increased in coculture-grown motor neurons as compared to control monocultures. Moreover, in coculture-grown motor neurons among motile mitochondria the percentage of anterograde shifts as compared to retrograde is significantly higher ($n = 9$ analyzed fields from 3 independent experiments per condition, a minimum of 10 axons per field were analyzed). $^{*}p < 0.0172$, $^{**}p < 0.0018$, $^{***}p < 0.0001$.

3. Conclusion

In this study, we present a microfluidic coculture system suitable for morphologic and functional analysis that resulted in the formation of bona fide human NMJs, in both physiological and pathological conditions. In the development of this system, we employed motor neurons derived from human iPSCs, which already demonstrated to be a promising cell source for in vitro patient-specific studies.[36,37] Under our experimental conditions, human motor neurons demonstrated proper differentiation and polarization through the expression of key neural markers and showing an electrophysiological profile typical of mature motor neurons (Figure 1). During the set-up phase, motor neurons were cocultured in the two-compartment microfluidic device together with skeletal muscle-derived hMSCs, which exhibited a great myogenic capability in our experiments (Figure 2A,B). iPSCs-derived neural progenitors and hMSCs were able to successfully establish mature coculture with differentiated motor neurons and myotubes forming contact points colocalizing with the major synaptic vesicle protein synaptophysin and the AChRs (Figures 5 and 6). The influence of muscle cells on motor neuron physiology have proved evident in two significant aspects: i) the total absence of neural projections in the distal compartment of control chips where only muscle growth medium was present, suggesting that differentiated myotubes are able to secrete factors attracting axons and promoting their growth (as reported also in literature);[15] ii) a marked increase in mitochondrial motility and their net anterograde shift in the axoplasm of coculture-grown motor neurons (Figure 7). In line with what was reported in the literature, the transport of mitochondria in the direction of the growth cone is more likely to be ascribed to a shift toward the highest metabolic demand region where the active growth of axons and the formation of the NMJ occur.[31,38]

Subsequently, considering the validation of the microfluidic coculture system on a diseased phenotype a fundamental need to assess the model relevance, we employed immortalized myoblasts from patients suffering from α-sarcoglycanopathy, a

© 2022 The Authors. Advanced Materials Technologies published by Wiley-VCH GmbH

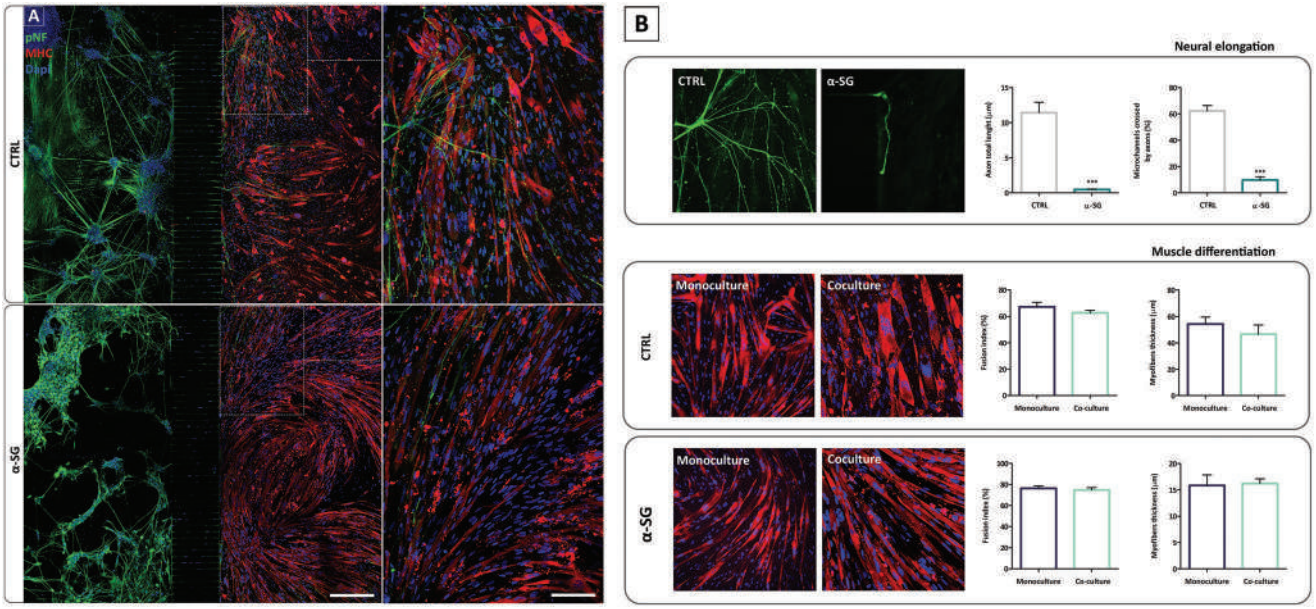

Figure 8. Human motor neurons and patient-derived immortalized myoblasts coculture in the two-compartment microfluidic chip. A) Representative immunostaining images of cocultures composed of healthy iPSCs-derived motor neurons and immortalized myoblasts from either healthy donors (CTRL) or α-SG patients. Each large image is sided by a magnified field of the region with the highest interaction between motor neurons and myotubes. Large images scale bar: 400 μm. Magnified fields scale bar: 200 μm. B) Evaluation of the neural elongation as axon total length 0.3 mm^{-2} and percentage of microchannels crossed by axons in CTRL and α-SG cocultures. Muscle differentiation analysis comparing fusion index and myotubes thickness derived from CTRL and α-SG myoblasts in control monoculture and in coculture with motor neurons ($n = 9$ analyzed fields from 3 independent experiments per condition). For myotubes thickness analysis a minimum of 10 myotubes per field were analyzed. ***$p < 0.0003$.

subtype of autosomal recessive limb-girdle muscular dystrophy. In fact, since the α-sarcoglycan protein was recently described to have a possible role in the NMJ stabilization during aging,[24] its lack in the affected patients may have consequences in the NMJ stability. Moreover, while the NMJ is being increasingly studied and characterized in the Duchenne Muscular Dystrophy,[21] the contribution of the NMJ to the α-sarcoglycanopathy pathology progression is still largely unknown. The first experiments clarified that both healthy and α-SG myoblasts were able to fuse and differentiate with high efficiency (Figure 2A,B). However, a morphological difference between healthy and α-SG myotubes emerged, generating significantly thinner fibers with fewer nuclei (between 2 and 5) in the pathological condition (Figure 2C,D).

We used the microfluidic coculture system to investigate whether a crosstalk occurs between muscle cells and motor neurons and if this equilibrium can be altered in pathological conditions. In particular, we employed pathological cells to disclose the specific role of the cellular components in the maturation of the NMJ. While motor neurons presence did not show any significant role in muscle differentiation efficiency, the effect of muscle cells on axons attraction and growth appeared evident. In fact, while myotube size in healthy and pathological cocultures was not affected by motor neurons presence (Figure 8B), α-SG myotubes performed far worse than their healthy counterpart in attracting motor neurons and promoting axons growth through microchannels. This effect was pointed out by a significantly lower percentage of microchannels occupied by axons and a lower axons total length in the presence of diseased myotubes (Figure 8B). It should be noted that – in healthy cocultures – motor neurons projections covered distances in the order of millimeters (Figure 8A). These data suggest that muscle cells genetic background and phenotype affects motor neuron recruitment. Also, an effect of the diseased phenotype on mitochondria motility directionality emerged that could be involved with the poor extent of axonal outgrowth: while in the healthy model the net anterograde mitochondria transport can be correlated with active growth and synapses formation, in the diseased model no predominant directionality was observed (Figure S3, Supporting Information). Further experiments aimed at exploring whether these phenomena are due to the active secretion of factors that impair axons growth or to the lower maturity reached by α-SG myoblasts derived myotubes are now warranted.

Although synaptophysin-AChRs colocalization has often been considered sufficient to assert the formation of NMJs in vitro,[15] in our opinion a further relevant confirmation should be considered the AChRs clustering, which is a key aspect of NMJ development. During the myogenic compartment characterization, muscle progenitors (both hMSCs and immortalized myoblasts) already displayed the prepatterning of the AChRs on the sarcolemma, revealing the ability of reproducing in vitro the first fundamental stage of the NMJ development, known to occur independently from neural signals (Figure 3).[28] In order to verify whether the interaction with motor neurons would actually result in the aggregation of the AChRs at the contact points, the density of prepatterned AChRs on monoculture myotubes was compared with the density of AChRs on myotubes interacting with motor neurons in microfluidic cocultures. A more pronounced cluster aggregation was found in

© 2022 The Authors. Advanced Materials Technologies published by Wiley-VCH GmbH

2365709x, 2022, 7, Downloaded from https://onlinelibrary.wiley.com/doi/10.1002/admt.202101216 by CochraneItalia, Wiley Online Library on [06/12/2024]. See the Terms and Conditions (https://onlinelibrary.wiley.com/terms-and-conditions) on Wiley Online Library for rules of use; OA articles are governed by the applicable Creative Commons License

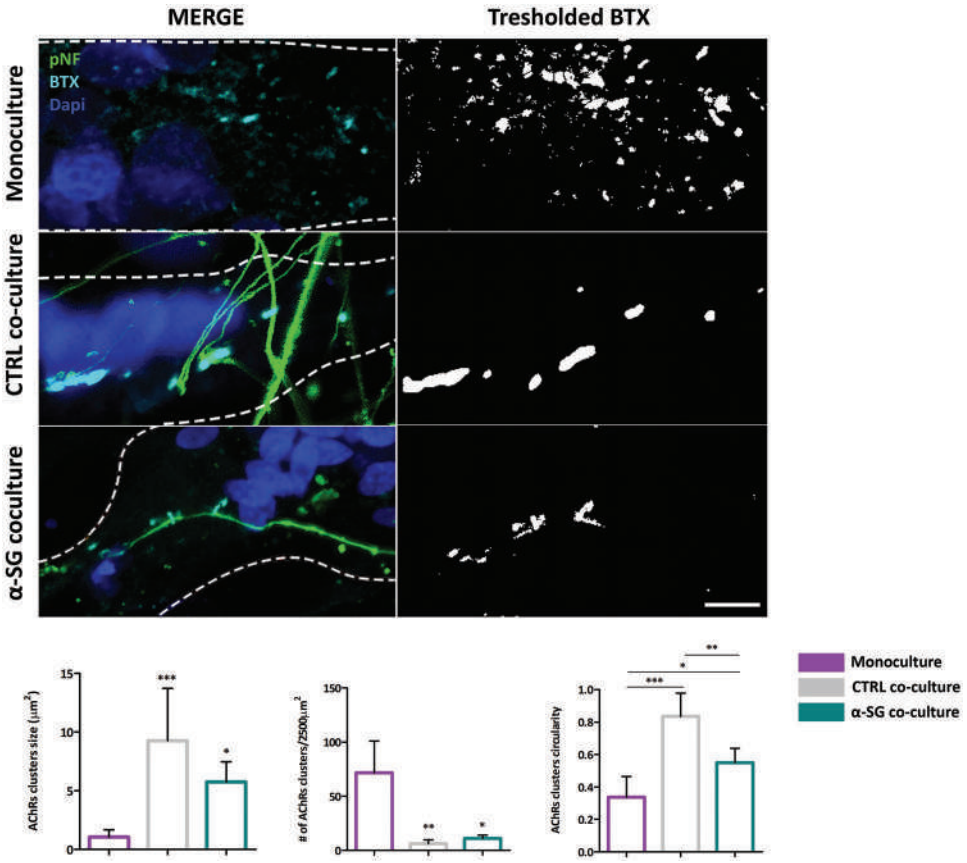

Figure 9. AChRs clustering analysis. Representative immunostaining images focusing on the sarcolemma of myotubes grown either in control monoculture, in CTRL coculture or in α-SG coculture. Dashed lines trace myotube outline. By converting the BTX-fluorescent signal in binary thresholded images, the density and the morphology of AChRs clusters were calculated as receptor clusters size, number of AChRs/2500 µm^2 and clusters circularity in all three conditions. Scale bar: 10 µm ($n = 9$ analyzed fields from 3 independent experiments per condition, a minimum of 10 myotubes per field were analyzed). One-way ANOVA Tukey's Multiple Comparison Test was performed. *$p < 0.05$, **$p < 0.001$, ***$p < 0.0001$.

cocultured myotubes resulting in significantly fewer but larger clusters, with an intermediate effect (although not statistically significant) in α-SG cocultures as compared to healthy cocultures (Figure 9). Moreover, we evaluated the circularity index of the AChRs clusters obtained in healthy and α-SG cocultures in order to verify whether they resembled the nummular structure described for the human NMJ.[4] This experiment clarified that coculture experiments yielded more defined AChRs clusters as compared to monocultures, with a significant difference being also detected between healthy and diseased myotubes. Our results demonstrate that the contact of myotubes with motor neurons in microfluidic cocultures exert a strong and direct effect on AChRs clustering, which overall appears slightly more efficient in CTRL as compared to α-SG cocultures. Moreover, together with the evidence that synaptophysin and bungarotoxin colocalized at the myotubes membrane, AChRs clustering provides an indication that bona fide human NMJs might be formed in our experimental model in both healthy and diseased models.

Overall the presented data show that skeletal muscle deeply influences motoneuron axon outgrowth and NMJ formation while conversely motoneurons do not affect myoblast differentiation and maturation capabilities.

4. Experimental Section

Isolation, Cell Culture, and Differentiation of Skeletal Muscle-Derived hMSCs: Skeletal muscle biopsies were obtained from healthy donors following informed consent in line with the guidelines of the Helsinki declaration on human rights. hMSCs were isolated from skeletal muscle biopsies using a protocol that involves mechanical mincing, enzymatic digestion with type II collagenase, filtration, and selection of the colonies on plastic surface at low confluence, as previously described.[26] Briefly, human skeletal muscle biopsies from healthy donors were finely minced with a surgical knife and collected in a solution of collagenase type II (100 U mL^{-1} in PBS Ca2+/Mg2+), subsequently incubated in a thermal shaker for 45 min at 37 °C. After digestion, the solution was centrifuged at 300 g for 10 min at room temperature (RT) and then aspirated without disturbing the pellet. The pellet was then resuspended in 15 mL of PBS and filtered through progressively finer cell strainers with 100, 70, and 40 µm mesh pores size. Cells were counted with a Burker counting chamber and plated on conventional Petri dishes (BD Falcon) at low confluence (103 cells cm^{-2}) to promote the growth of cells that had clonogenicity and therefore stem potentiality. Freshly isolated hMSCs were cultured in Cyto-Grow medium (Resnova) supplemented with penicillin (100 IU mL^{-1}, Gibco) and streptomycin (100 mg mL^{-1}, Gibco) at 37 °C and 5% CO_2 and incubated for 15 days, the time required for colonies formation. Cyto-grow, an enriched growth medium, has previously been reported to have a better efficiency in maintaining myogenic capabilities on primary human stem cells with mesenchymal

© 2022 The Authors. Advanced Materials Technologies published by Wiley-VCH GmbH

2365709x, 2022, 7, Downloaded from https://onlinelibrary.wiley.com/doi/10.1002/admt.202101216 by CochraneItalia, Wiley Online Library on [06/12/2024]. See the Terms and Conditions (https://onlinelibrary.wiley.com/terms-and-conditions) on Wiley Online Library for rules of use; OA articles are governed by the applicable Creative Commons License

derivation.[26] After colonies formation, cells were expanded for both differentiation analysis and cocultures experiments. In particular, differentiation was achieved spontaneously once the culture reached a cell confluence of 80%, without needing differentiation medium or specific factors.

Cell Culture and Differentiation of hTERT/CDK4 Human Immortalized Myoblasts: hTERT/CDK4 human immortalized myoblasts from healthy donors and α-sarcoglycanopthy-suffering patients were kindly provided by Dr. V. Mouly group.[39] Undifferentiated myoblasts were cultured in F12 (Gibco) supplemented with 20% heat-inactivated fetal bovine serum (FBS, EuroClone), 100 IU mL^{-1} penicillin (Gibco), 100 mg mL^{-1} streptomycin (Gibco), 25 µg mL^{-1} fetuin, 0.5 ng mL^{-1} bFGF, 5 ng mL^{-1} EGF, 5 µg mL^{-1} insulin, 0.2 µg mL^{-1} dexamethasone. Cells were expanded for both differentiation analysis and coculture experiments. Differentiation was achieved once the culture reached 80% confluence by induction with differentiation medium, composed by DMEM and 10 µg mL^{-1} insulin.

Spinal Motor Neurons Differentiation From Human iPSCs: Motor neurons were differentiated from human iPSCs with an adapted feeder-free version of a well-established transgene-free protocol. Briefly, iPCSs derived from healthy donor were plated on Matrigel-coated Petri dishes (BD Falcon) and cultured in Essential 8 medium (xeno-free and feeder-free medium, Gibco) at 37 °C and 5% CO_2 to allow colony formation. When colonies reached optimal size, they were detached with dispase (1 U mL^{-1}, Gibco), transferred to 25 cm^2 flasks (differentiation day 0) and grown in suspension to allow embryoid bodies formation. Embryoid bodies were maintained in Essential 6 medium (xeno-free and feeder-free medium, Gibco) for the first 4 days, and then switched to neural induction medium (NIM; DMEM/F12, 1% N_2 supplement, 1% nonessential amino acids, 280 UI mL^{-1} heparin, and 1% penicillin–streptomycin) to promote differentiation toward the neural line. At differentiation day 10, embryoid bodies were transferred to laminin-coated six-well plates for neural rosettes formation. At differentiation day 15, the neural rosettes were picked and transferred to 25 cm^2 flasks and grown in suspension with NIM complete medium (NIM, 2% B27 supplement, 200 ng mL^{-1} ascorbic acid) with the addition of 100×10^{-9} M retinoic acid (RA) and 100 ng mL^{-1} sonic hedgehog (SHH) for up to 2 weeks, refreshing the medium every other day. Neural spheroids were picked and dissociated by accutase (Gibco) and trypsin/EDTA (EuroClone) treatment for 15 min and the suspension was centrifuged at 180 g for 5 min at RT. The pellet was washed with DMEM/F12 and resuspended in neural optimized medium complete (NOM; Neurobasal, 1% N2 supplement, 2% B27 supplement, and 1% penicillin–streptomycin, 10 ng mL^{-1} BDNF, 10 ng mL^{-1} GDNF, 10 ng mL^{-1} bFGF, 100×10^{-9} M cAMP, 200 ng mL^{-1} ascorbic acid) with the addition of 50×10^{-9} M RA and 50 ng mL^{-1} SHH. Finally, the obtained progenitors were plated either over Matrigel-coated coverslips into 24-well plates (for immunofluorescence analysis) or into Matrigel-coated 96-well multielectrode arrays-plates (for electrophysiology analysis, see below). Alternatively, neural progenitors were employed for coculture experiments.

Cell Culture in the Microfluidic Chip: Microfluidic chips were sterilized by rinsing PDMS devices with 70% ethanol and allowed to dry in a sterile environment (30 min), as per the user manual instructions (Xona Microfluidics, RD450). Subsequently, microfluidic chips were mounted on sterile glass coverslips by gentle pressure and both cell culture compartments were coated with Matrigel for 2 h at 37 °C. Coating was removed and substrates were washed with PBS in preparation of cell seeding. Muscle progenitors (either hMSCs or immortalized myoblasts) were harvested and seeded first in the distal chamber at a concentration of 1×10^5 per compartment. After about 30 min, needed to allow muscle cells attachment to the substrate, motor neurons progenitors were harvested from neural spheroids and seeded in the proximal chamber at a concentration of 1.8×10^5 per compartment. In the control chips, only motor neurons have been cultured in the proximal compartment, with the distal compartment being filled with muscle medium only. Devices were then incubated for 1 h at 37 °C to facilitate cell attachment, followed by the addition of their respective media to fill devices. Immortalized myoblasts differentiation was initiated after 3 days of proliferation by adding myoblasts differentiation medium (see above), while motor neurons were fluidically isolated and maintained in NOM complete medium supplemented with 50×10^{-9} M RA and 50 ng mL^{-1} SHH throughout the entire duration of the experiment. Motor neurons fluidic isolation was achieved by maintaining a larger volume of medium in the reservoirs of the neural compartment and was favorable to create a slight mechanical force to promote axons growth through microchannels and, most importantly, to make sure that the demanding differentiation of motor neurons was not altered by the influence of muscle medium. Media were changed daily. Once motor neurons had contacted myotubes and a mature coculture was established by day 15, the experiment was interrupted to proceed to further analysis. Neural and muscle cells growth was monitored daily on a Nikon Eclipse Ts2 equipped with a HD Digital Camera (TP1080HDMI).

Immunofluorescence Analysis: After rinsing media residues with PBS, cells plated for differentiation analysis and microfluidic chips cultures were fixed with 4% PFA in PBS at 4 °C for 10 and 30 min, respectively. In the case of microfluidic cultures, a longer incubation time and a larger liquid volume in the reservoirs of neural compartments were required to ensure that the fixing solution penetrated completely inside the microchannels. After fixation, cells were processed for immunofluorescence analysis as previously described.[26] Briefly, cells were permeabilized with Triton X-100 0.3% in PBS for 1 h at RT and blocked with a blocking solution consisting of 10% goat serum, 1% glycine, 0.1% Triton X-100 in PBS for 1 h at RT. Subsequently, cells were incubated with primary antibodies in blocking solution for 2 h at RT and then rinsed with a washing solution consisting of 1% BSA and 0.2% Triton X-100 in PBS. Primary antibodies were diluted as follows: rabbit polyclonal anti-HB9 (Abcam) 1:200, mouse monoclonal anti-HB9 (Santa Cruz Biotechnology) 1:100, mouse monoclonal anti-pNF (BioLegend) 1:800, rabbit polyclonal anti-pNF (BioLegend) 1:400, mouse monoclonal anti-NeuN (Millipore) 1:200, rabbit polyclonal anti-MAP2 (Abcam) 1:800, mouse polyclonal anti-GFAP (Millipore) 1:500, rabbit monoclonal anti-Tau (Dako) 1:800, mouse monoclonal anti-MHC (MF20, DHSB) 1:2, mouse monoclonal anti-βIII tubulin (Santa Cruz Biotechnology) 1:100, rabbit polyclonal anti-desmin (Abcam) 1:100, mouse monoclonal anti-synaptophysin (Abcam) 1:100. After washing, cells were incubated with Alexa Fluor 555-conjugated goat anti-mouse IgG (H + L; Thermo Fisher Scientific, diluted 1:400) and 488-conjugated goat anti-rabbit IgG (H + L; Thermo Fisher Scientific, diluted 1:400) for 1 h. Finally, nuclei were stained with 300×10^{-9} M DAPI (Thermo Fisher Scientific) in PBS for 30 min. When fluorescent-BTX staining was needed, α-BTX Alexa Fluor 488-conjugated or α-BTX Alexa Fluor 647-conjugated were added to DAPI solution at a concentration of 1:400. Specimens were visualized using a Nikon TE 2000 epifluorescence microscope equipped with a Photometrics Cool SNAP MYO CCD camera and images were acquired through MetaMorph software (Molecular Devices, Inc.). Alternatively, images were acquired through a Nikon A1R laser scanning confocal microscope with the NIS software (Tissue Engineering Unit, "Campus Biomedico" University, Rome, Italy).

Image Analyses: The AChRs Clustering: In order to describe AChRs clustering on the myotubes sarcolemma, highly magnified confocal images of fluorescent BTX-binding AChRs were processed and analyzed through the ImageJ program. The acquired fluorescent BTX signal was converted in highly contrasted 8-bit images and threshold = 50 was applied to generate binary images. After having calibrated the scale of the image and having set the measurements of interest, number, size, and circularity of the clusters were obtained through the Analyze Particles function (Analyze > Analyze Particles).

MitoTracker Analysis: To study mitochondrial motility in the axoplasm, mitochondria were labeled with MitoTracker Green FM (Invitrogen). For this purpose, on day 15 of coculture, the media in the reservoirs of neural compartment of the control chips and of the microfluidic cocultures were replaced with a solution of 100×10^{-9} M MitoTracker in NOM complete medium. Cells were incubated at 37 °C for 15 min to allow

© 2022 The Authors. Advanced Materials Technologies published by Wiley-VCH GmbH

2365709x, 2022, 7, Downloaded from https://onlinelibrary.wiley.com/doi/10.1002/admt.202101216 by CochraneItalia, Wiley Online Library on [06/12/2024]. See the Terms and Conditions (https://onlinelibrary.wiley.com/terms-and-conditions) on Wiley Online Library for rules of use; OA articles are governed by the applicable Creative Commons License

the fluorescent probe to bind mitochondria in the axons. After staining was complete, the staining solution was replaced by fresh prewarmed medium and cells were observed with a Nikon TE 2000 epifluorescence microscope. Mitochondrial dynamics in live cells was recorded through time-lapse images (an image was acquired every 10 s for 10 min) using MetaMorph software. Images were acquired at the interface between the neural compartment and the microchannels entrance to make sure to include in the analysis axons growing through the microchannels and communicating with the distal compartment. Kymographs obtained from the recordings through the KymographBuilder ImageJ plug-in were utilized for the calculation of mitochondrial velocity, mitochondrial shift length, motile mitochondria percentage, and anterograde shift percentage.

MEA Analysis: During the characterization phase, motor neurons functionality was evaluated through MEA analysis (Center for Translational Medicine, International Clinical Research Center, FNUSA, Brno, Czech Republic). For this purpose, 10–12 µL of Matrigel were placed on the electrodes in the center of each well of a 96-well multielectrode array plate then incubated at 37 °C for 2 h. Subsequently, Matrigel was removed and the iPSCs-derived motor neurons progenitors – resuspended in a volume of 10–12 µL – were seeded in each well at a concentration of 5×10^4 per well. After a 30 min incubation to promote cell attachment, each well was filled with 200 µL of NOM complete medium with the addition of 50×10^{-9} M RA and 50 ng mL^{-1} SHH. Motor neurons maturation was carried out for up to 30 days. Local field potentials of electrically active cells were recorded daily using the MAESTRO MEA Axion Biosystem and data were acquired through the Neural Module software.

Statistical Analysis: All experiments were performed in biological and technical triplicate. Data were analyzed using GraphPad Prism 5, and values were expressed as means ± standard error (SEM). Statistical significance was tested using either ONE WAY ANOVA and Tukey's post hoc test or *t*-test when only two parameters were compared. A probability of less than 5% ($p < 0.05$) was considered to be statistically significant.

Supporting Information

Supporting Information is available from the Wiley Online Library or from the author.

Acknowledgements

The authors thank the platform for immortalization of human cells from the Institut de Myologie, GH Pitié-Salpétrière for providing immortalized myoblasts. They also thank Dr. Franca Abbruzzese (Università Campus Bio-Medico di Roma) for her valuable technical support on confocal microscopy acquisition. The research has been carried out thanks to PRIN 2017: 201742SBXA_004 founded by Italian Ministry of University and Research to Cesare Gargioli. Giancarlo Forte, was supported by the European Social Fund and European Regional Development Fund-Project MAGNET (CZ.02.1.01/0.0/0.0/15_003/0000492).

Conflict of Interest

The authors declare no conflict of interest.

Data Availability Statement

The data that support the findings of this study are available in the supplementary material of this article.

Keywords

microfluidic, muscle dystrophy, neural muscular junction, NMJ modeling, organ on a chip

Received: October 12, 2021
Revised: December 22, 2021
Published online: March 17, 2022

[1] R. R. Nair, S. Corrochano, S. Gasco, C. Tibbit, D. Thompson, C. Maduro, Z. Ali, P. Fratta, A. A. Arozena, T. J. Cunningham, E. M. C. Fisher, *Mamm. Genome* **2019**, *30*, 173.
[2] A. Natarajan, A. Sethumadhavan, U. M. Krishnan, *ACS Omega* **2019**, *4*, 12969.
[3] V. Picher-Martel, P. N. Valdmanis, P. V. Gould, J. P. Julien, N. Dupré, *Acta Neuropathol. Commun.* **2016**, *4*, 70.
[4] R. A. Jones, C. Harrison, S. L. Eaton, M. Llavero Hurtado, L. C. Graham, L. Alkhammash, O. A. Oladiran, A. Gale, D. J. Lamont, H. Simpson, M. W. Simmen, C. Soeller, T. M. Wishart, T. H. Gillingwater, *Cell Rep.* **2017**, *21*, 2348.
[5] M. Das, J. W. Rumsey, N. Bhargav, M. Stancescu, J. J. Hickman, *Biomaterials* **2010**, *31*, 4880.
[6] J. A. Umbach, K. L. Adams, C. B. Gundersen, B. G. Novitch, *PLoS One* **2012**, *7*, 3.
[7] J. W. Santoso, M. L. McCain, *DMM Dis. Model. Mech.* **2020**, *13*, https://doi.org/10.1242/dmm.044867.
[8] J. W. Park, B. Vahidi, A. M. Taylor, S. W. Rhee, N. L. Jeon, *Nat. Protoc.* **2006**, *1*, 2128.
[9] A. Ionescu, E. E. Zahavi, T. Gradus, K. Ben-Yaakov, E. Perlson, *Eur. J. Cell Biol.* **2016**, *95*, 69.
[10] H. S. Park, S. Liu, J. McDonald, N. Thakor, I. H. Yang, *Proc. Annu. Int. Conf. IEEE Eng. Med. Biol. Soc. EMBS* **2013**, 2833.
[11] K. A. Southam, A. E. King, C. A. Blizzard, G. H. McCormack, T. C. Dickson, *J. Neurosci. Methods* **2013**, *218*, 164.
[12] S. G. M. Uzel, R. J. Platt, V. Subramanian, T. M. Pearl, C. J. Rowlands, V. Chan, L. A. Boyer, P. T. C. So, R. D. Kamm, *Sci. Adv.* **2016**, *2*, https://doi.org/10.1126/sciadv.1501429.
[13] N. Santhanam, L. Kumanchik, X. Guo, F. Sommerhage, Y. Cai, M. Jackson, C. Martin, G. Saad, C. W. McAleer, Y. Wang, A. Lavado, C. J. Long, J. J. Hickman, *Biomaterials* **2018**, *166*, 64.
[14] Z. Tong, O. Seira, C. Casas, D. Reginensi, A. Homs-Corbera, J. Samitier, J. A. Del Río, *RSC Adv.* **2014**, *4*, 54788.
[15] E. E. Zahavi, A. Ionescu, S. Gluska, T. Gradus, K. Ben-Yaakov, E. Perlson, *J. Cell Sci.* **2015**, *128*, 1241.
[16] C. A. Blizzard, K. A. Southam, E. Dawkins, K. E. Lewis, A. E. King, J. A. Clark, T. C. Dickson, *DMM Dis. Model. Mech.* **2015**, *8*, 215.
[17] R. Mills, H. Taylor-Weiner, J. C. Correia, L. Z. Agudelo, I. Allodi, C. Kolonelou, V. Martinez-Redondo, D. M. S. Ferreira, S. Nichterwitz, L. H. Comley, V. Lundin, E. Hedlund, J. L. Ruas, A. I. Teixeira, *Mol. Metab.* **2018**, *7*, 12.
[18] K. Stoklund Dittlau, E. N. Krasnow, L. Fumagalli, T. Vandoorne, P. Baatsen, A. Kerstens, G. Giacomazzi, B. Pavie, E. Rossaert, J. Beckers, M. Sampaolesi, P. Van Damme, L. Van Den Bosch, *Stem Cell Rep.* **2021**, *16*, 2213.
[19] T. Osaki, S. G. M. Uzel, R. D. Kamm, *Sci. Adv.* **2018**, *4*, eaat5847.
[20] T. Osaki, S. G. M. Uzel, R. D. Kamm, *Nat. Protoc.* **2020**, *15*, 421.
[21] S. Y. Ng, V. Ljubicic, *EBioMed.* **2020**, *61*, 103032.
[22] Z. Xie, Y. Hou, M. Yu, Y. Liu, Y. Fan, W. Zhang, Z. Wang, H. Xiong, Y. Yuan, *Orphanet J. Rare Dis.* **2019**, *14*, 43.
[23] A. P. Murphy, V. Straub, *J. Neuromuscul. Dis.* **2015**, *2*, S7.
[24] K. Zhao, C. Shen, L. Li, H. Wu, G. Xing, Z. Dong, H. Jing, W. Chen, H. Zhang, Z. Tan, J. Pan, L. Xiong, H. Wang, W. Cui, X. D. Sun, S. Li, X. Huang, W. C. Xiong, L. Mei, *J. Neurosci.* **2018**, *38*, 8860.
[25] M. Santello, N. Toni, A. Volterra, *Nat. Neurosci.* **2019**, *22*, 154.

© 2022 The Authors. Advanced Materials Technologies published by Wiley-VCH GmbH

2365709x, 2022, 7, Downloaded from https://onlinelibrary.wiley.com/doi/10.1002/admt.202101216 by CochraneItalia, Wiley Online Library on [06/12/2024]. See the Terms and Conditions (https://onlinelibrary.wiley.com/terms-and-conditions) on Wiley Online Library for rules of use; OA articles are governed by the applicable Creative Commons License

[26] S. Testa, C. S. Riera, E. Fornetti, F. Riccio, C. Fuoco, S. Bernardini, J. Baldi, M. Costantini, M. L. Foddai, S. Cannata, C. Gargioli, *Front. Physiol.* **2020**, *11*, 553198.
[27] C. Mozzetta, S. Consalvi, V. Saccone, M. Tierney, A. Diamantini, K. J. Mitchell, G. Marazzi, G. Borsellino, L. Battistini, D. Sassoon, A. Sacco, P. L. Puri, *EMBO Mol. Med.* **2013**, *5*, 626.
[28] V. Witzemann, *Cell Tissue Res.* **2006**, *326*, 263.
[29] C. L. Happe, K. P. Tenerelli, A. K. Gromova, F. Kolb, A. J. Engler, *Mol. Biol. Cell* **2017**, *28*, 1950.
[30] L. Vernetti, A. Gough, N. Baetz, S. Blutt, J. R. Broughman, J. A. Brown, J. Foulke-Abel, N. Hasan, J. In, E. Kelly, O. Kovbasnjuk, J. Repper, N. Senutovitch, J. Stabb, C. Yeung, N. C. Zachos, M. Donowitz, M. Estes, J. Himmelfarb, G. Truskey, J. P. Wikswo, D. L. Taylor, *Sci. Rep.* **2017**, *7*, 44517.
[31] W. M. Saxton, P. J. Hollenbeck, *J. Cell Sci.* **2012**, *125*, 2095.
[32] M. Singh, H. Denny, C. Smith, J. Granados, R. Renden, *J. Physiol.* **2018**, *596*, 6263.
[33] J. Montes, A. M. Goodwin, M. P. McDermott, D. Uher, F. M. Hernandez, K. Coutts, J. Cocchi, M. Hauschildt, K. M. Cornett, A. K. Rao, U. R. Monani, C. Ewing Garber, D. C. De Vivo, *Ann. Clin. Transl. Neurol.* **2021**, *8*, 1086.
[34] M. A. Bakooshli, E. S. Lippmann, B. Mulcahy, N. Iyer, C. T. Nguyen, K. Tung, B. A. Stewart, H. Van Den Dorpel, T. Fuehrmann, M. Shoichet, A. Bigot, E. Pegoraro, H. Ahn, H. Ginsberg, M. Zhen, R. S. Ashton, P. M. Gilbert, *Elife* **2019**, *8*, e44530.
[35] C. Y. Lin, M. Yoshida, L. T. Li, A. Ikenaka, S. Oshima, K. Nakagawa, H. Sakurai, E. Matsui, T. Nakahata, M. K. Saito, *JCI Insight* **2019**, *4*, https://doi.org/10.1172/jci.insight.124299.
[36] M. Murdocca, S. A. Ciafrè, P. Spitalieri, R. V. Talarico, M. Sanchez, G. Novelli, F. Sangiuolo, *Int. J. Mol. Sci.* **2016**, *17*, 1231.
[37] S. Sances, L. Bruijn, S. Chandran, K. Eggan, R. Ho, J. Klim, M. Livesey, E. Lowry, J. Macklis, D. Rushton, C. Sadegh, D. Sareen, H. Wichterle, S. Zhang, C. Svendsen, *Nat. Neurosci.* **2016**, *19*, 542.
[38] C. W. Lee, H. B. Peng, *Mol. Biol. Cell* **2008**, *19*, 150.
[39] M. Thorley, S. Duguez, E. M. C. Mazza, S. Valsoni, A. Bigot, K. Mamchaoui, B. Harmon, T. Voit, V. Mouly, W. Duddy, *Skelet. Muscle* **2016**, *6*, 43.

© 2022 The Authors. Advanced Materials Technologies published by Wiley-VCH GmbH

2365709x, 2022, 7, Downloaded from https://onlinelibrary.wiley.com/doi/10.1002/admt.202101216 by CochraneItalia, Wiley Online Library on [06/12/2024]. See the Terms and Conditions (https://onlinelibrary.wiley.com/terms-and-conditions) on Wiley Online Library for rules of use; OA articles are governed by the applicable Creative Commons License